Scientific Reports

https://doi.org/10.1038/s41598-026-43340-y

Article in Press

Synergistic adsorption of NH_3 and H_2S over layered hydrochar-derived pyrochars: mechanistic divergence and cooperative acid-base activation

Received: 2 January 2026

Accepted: 3 March 2026

Published online: 17 March 2026

Cite this article as: Ko M. & Ko J.H. Synergistic adsorption of NH_3 and H_2S over layered hydrochar-derived pyrochars: mechanistic divergence and cooperative acid-base activation. *Sci Rep* (2026). https://doi.org/10.1038/s41598-026-43340-y

Myeongjin Ko & Jae Hac Ko

Synergistic Adsorption of NH_3 and H_2S over Layered Hydrochar-Derived Pyrochars: Mechanistic Divergence and Cooperative Acid-Base Activation

Myeongjin Ko[1], Jae Hac Ko [1,*]

[1]Department of Environmental Engineering, Jeju National University
102 Jejudaehak-ro, Jeju-si, Jeju Special Self-Governing Province, 63243, Republic of Korea
[*] Corresponding author, Email address: jaehacko@jejunu.ac.kr, 0000-0002-0990-364X

Abstract: NH_3 and H_2S are major hazardous odorants emitted from intensive livestock operations, presenting distinct challenges for simultaneous removal. This study evaluates a novel layered filtration system utilizing swine-manure-derived pyrochars produced via a two-stage hydrothermal carbonization (HTC) and pyrolysis process. Chars produced at 350 °C (PMB350) and 550 °C (PMB550) exhibited divergent physicochemical properties. Increasing pyrolysis temperature increased BET surface area (27.94 to 90.00 m^2 g^{-1}) and alkalinity (pH 8.59 to 9.80), while reducing oxygenated surface functionalities. In single-gas fixed-bed tests (100 ppm; 100 mL min^{-1}), PMB350 exhibited higher NH_3 capacity (7.10 mg g^{-1}) than PMB550 (4.86 mg g^{-1}), consistent with Brønsted acid–base capture to form surface NH_4^+. In contrast, PMB550 showed substantially higher H_2S capacity (9.70 mg g^{-1}) than PMB350 (2.54 mg g^{-1}), reflecting the combined influence of pore development and mineral/alkaline sites. Layered beds (0.25 g + 0.25 g) provided mixed-gas performance (NH_3 + H_2S, each 100 ppm) with H_2S capacities of 7.15-7.60 mg g^{-1} depending on bed order. X-ray photoelectron spectroscopy (XPS) analysis revealed that co-adsorbed NH_3 functioned as a surface activator, enhancing the oxidative conversion of H_2S to sulfate in the acidic upstream layer (PMB350) and amplifying sulfur mineralization in the alkaline downstream layer (PMB550). The synergy is attributed to an in-situ surface alkalinization mechanism where adsorbed NH_3 facilitates H_2S dissociation. These findings demonstrate that spatially arranging sorbents with complementary acid-base properties can exploit cooperative chemical interactions, offering a sustainable, high-efficiency strategy for complex odor mitigation.

Highlights

- Layered hydrochar-pyrochars enable synergistic removal of NH_3 and H_2S.
- Acidic char captures NH_3, while alkaline char facilitates H_2S mineralization.
- Stacking these two pyrochar layers created a synergy: NH_3 actually helped trap much more H_2S.
- Adsorbed NH_3 induces surface alkalinization, promoting H_2S oxidation.

Graphical abstract

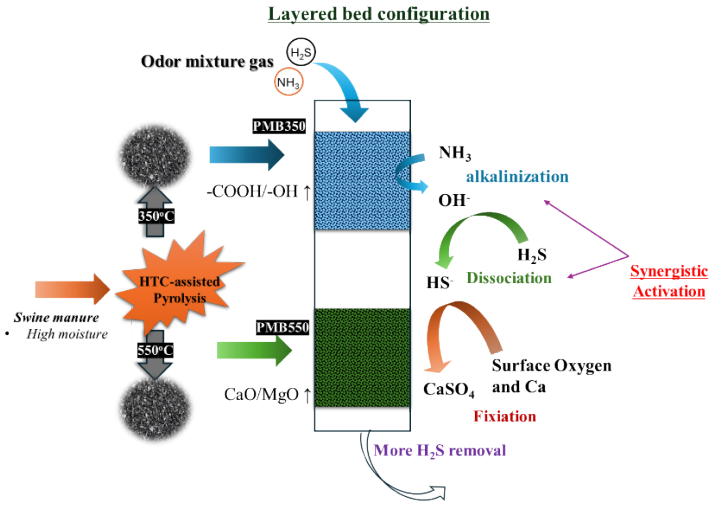

Keywords: swine manure; hydrothermal carbonization; pyrochar; ammonia; hydrogen sulfide; layered bed

1 Introduction

The intensification of livestock production systems globally has exacerbated the emission of odorous and toxic gases, presenting severe environmental and occupational health challenges. Among these emissions, ammonia (NH_3) and hydrogen sulfide (H_2S) are frequently identified as key contributors to odor nuisance and acute exposure risk, motivating the development of practical control technologies for both point and area sources (Song 2024).

Biochar, a porous carbonaceous material produced from the thermochemical conversion of biomass, has emerged as a sustainable adsorbent for air pollution control. Utilizing swine manure as a feedstock for biochar production aligns with the principles of the circular economy, transforming a problematic high-nutrient waste into a value-added environmental remediation tool (Ayaz et al. 2025; Ravindiran et al. 2024). A major practical barrier to thermochemical stabilization of swine manure is its high moisture content, commonly in the 80-90 % range, which makes direct dry pyrolysis energy-inefficient due to the large latent heat required to evaporate water. Hydrothermal carbonization (HTC) offers a wet-processing route that converts high-moisture biomass into a carbon-rich solid (hydrochar) in hot compressed water, thereby avoiding a separate drying step. HTC can rapidly densify wet manure, reduce bulk volume, and partially stabilize odor-causing organics. However, hydrochars commonly exhibit limited surface area and porosity, which can constrain their direct use as gas adsorbents (Ighalo et al. 2022).

In practice, very wet feedstocks can be uneconomical to pyrolyze because of the costly pre-drying required. This challenge necessitates alternative approaches that can process wet biowaste without drying, thereby improving overall energy efficiency. HTC is one such solution: it carbonizes high-moisture biomass in hot compressed water (typically 180–240 °C under autogenous pressure), eliminating the need for a separate drying step (Ipiales et al. 2023; Wang et al. 2018). In an HTC process, swine manure can be converted within hours into a coal-like solid called hydrochar, drastically reducing the feedstock's moisture, volume, and odor (Fang et al. 2018). This fast "wet-to-solid" conversion curbs malodorous emissions early and yields a densified char product. Cavali et al. (2023) noted that the resulting hydrochar can serve as a functional sorbent for environmental applications, capable of removing pollutants from water, soil, and even air. However, raw hydrochar often has low surface area and porosity, which limits its efficacy for adsorbing gases or odors without further treatment.

To overcome these structural limitations, integrating HTC as a pretreatment prior to ha gained attention. The HTC step substantially reduces the moisture content and volatile matter of the feed, which in turn lowers the heat demand in the subsequent pyrolysis stage. Studies have shown that coupling HTC with pyrolysis can significantly reduce energy consumption compared to direct pyrolysis (Olszewski et al. 2020). For instance, the HTC process obviates a drying step and has been reported to save on the order of 50 % of energy relative to conventional drying-plus-pyrolysis approaches (Maniscalco et al. 2020). Beyond energy efficiency, the two-step process improves the material properties of the final char. During pyrolysis of the hydrochar, the residual volatiles are released, causing structure shrinkage and pore formation that greatly increase the surface area compared to one-step pyrolysis char. Garlapalli et al. (2016) observed, for example, that a pyrochar produced at 800 °C after HTC had about 5.5 times larger BET surface area than the original hydrochar. Correspondingly, HTC-assisted pyrochars tend to achieve higher fixed carbon and lower ash content than chars from single-step pyrolysis. These structural and compositional improvements can enhance interactions with a broad spectrum of gas-phase pollutants. Zhao et al. (2022b) emphasized that a large surface area, well-developed porosity, and abundant surface functional groups are key attributes for adsorbents in air pollution control.

The malodorous gases from livestock manure span multiple chemical groups - reduced sulfur compounds (e.g., H_2S, CH_3SH), nitrogen compounds (e.g., NH_3, trimethylamine), volatile organic compounds (VOCs), and volatile fatty acids (VFAs) (Marszałek et al. 2018). These gases are generated mainly by anaerobic decomposition in manure and can be detected even at trace levels owing to low odor thresholds (Wang et al. 2021). When attempting to remove such contaminants, multicomponent effects must be considered. Recent studies highlight that surface chemistry and co-adsorbates can strongly influence competitive adsorption from mixed gases (Jiang et al. 2022; Su et al. 2023; Zeng et al. 2024). Jiang et al. (2022) demonstrated that NH_3 uptake on carbonaceous sorbents depends on oxygenated acidic groups, whereas H_2S removal relies on mineral/alkaline sites. In mixed streams, H_2S can occupy or neutralize some of those acidic sites, leading to suppressed NH_3 adsorption when both gases compete for overlapping binding sites. Su et al. (2023) further reported that the presence of co-adsorbed water and the overall surface acidity/basicity can alter NH_3 adsorption pathways, underscoring the sensitivity of NH_3 uptake to sorbent surface conditions. Zeng et al. (2024) observed that on certain sorbents the redistribution of surface charge under dual-gas conditions can shift competitive adsorption routes and even reverse the selectivity between co-existing species. These findings collectively suggest that an ideal sorbent for mixed malodorous gases should integrate complementary binding mechanisms to effectively handle both NH_3 and H_2S simultaneously.

Numerous adsorbents have been explored for NH_3 and H_2S removal, but each exhibits inherent limitations. Impregnated activated carbons provide high capacity yet suffer from moisture-induced pore blockage and poor regenerability (de Oliveira et al. 2019; Guo et al. 2007; Mohamed et al. 2024). Metal oxides are highly reactive toward H_2S but show weak NH_3 affinity and require high-temperature regeneration (Khabazipour & Anbia 2019). Zeolite and metal-organic frameworks (MOFs) offer tunable adsorption but are hindered by competitive water adsorption and moisture instability (DeCoste & Peterson 2014; Pérez-Botella et al. 2022). These contrasts indicate that a single material struggles to simultaneously capture acidic and basic gases. Waste-derived pyrochars, whose acid-base properties can be tuned by temperature, offer a low-cost alternative.

Most previous studies on biochar-based removal of NH_3 and H_2S have focused on improving individual sorbents through material modification or evaluating adsorption under single-gas conditions (Bhoria et al. 2020; Zhuang et al. 2021). Even in multicomponent systems, adsorption behavior is typically interpreted in terms of site competition, surface neutralization, or inhibition occurring on a single sorbent surface. Because these approaches attempt to accommodate distinct adsorption mechanisms within the same chemical environment, control over simultaneous removal performance

remains limited.

Thus, the key challenge is not only to understand multicomponent adsorption behavior but also to determine how complementary surface chemistries should be spatially organized within an adsorption bed to regulate reaction sequence and interaction pathways. In particular, systematic design of layered sorbent architectures exploiting acid-base complementarity remains largely unexplored compared with conventional single-sorbent or blended-sorbent strategies.

To address this gap, a layered-bed configuration constructed from swine manure-derived chars produced via HTC-assisted pyrolysis at different temperatures is proposed. The low-temperature pyrochar retains oxygen-containing acidic functional groups favorable for NH_3 adsorption, whereas the high-temperature pyrochar provides alkaline/mineral sites that enhance H_2S capture. Spatial arrangement of these complementary sorbents within a single column is expected to induce cooperative removal behavior rather than independent adsorption.

Hydrochar-assisted pyrolysis chars were produced at two final temperatures and evaluated their individual adsorption performance toward NH_3 and H_2S. A layered bed configuration was subsequently tested by packing the low-temperature and high-temperature pyrochars to treat a mixed NH_3-H_2S gas stream under controlled conditions. All experiments were carried out with dry standard gases under air-free conditions (N_2 balance gas) to eliminate moisture or oxidative side reactions, thereby enabling a clearer interpretation of the intrinsic gas-sorbent interactions. Pre- and post-adsorption characterizations (e.g., surface functional groups and speciation of adsorbed sulfur/nitrogen) were performed to elucidate the removal mechanisms in the single-layer and layered systems.

2. Materials and Methods

As shown in Fig. 1, the overall experimental procedure consisted of sample collection, hydrothermal carbonization (HTC), pyrolysis, and adsorption experiments; the detailed

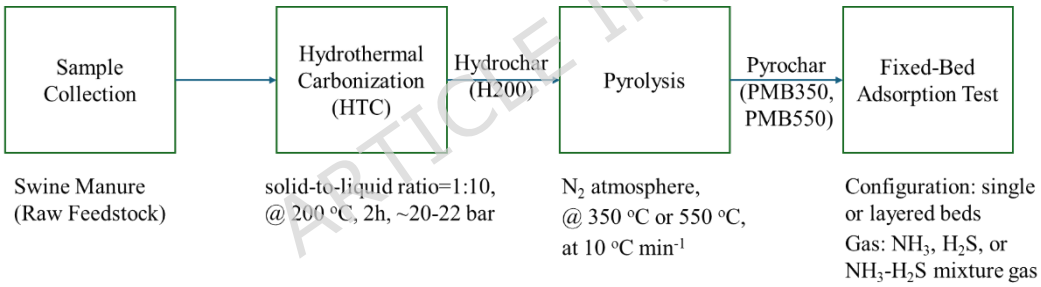

methods are described below.

Fig. 1. Flow chart of experimental procedure.

2.1 Biochar Production

Swine manure was collected from a swine farm in Hallim-eup, Jeju. The manure was centrifuged to separate solid and liquid fractions, and the recovered solid fraction was used as the HTC reaction medium. The mixture was prepared at a solid-to-liquid ratio of 1:10 (total volume 1.1 L) using D.I water, was subjected to HTC at 200 °C for 2 h (heating rate 5 °C min^{-1}) in a sealed reactor, reaching an internal pressure of ~20-22 bar. After cooling to room temperature, the solid and liquid phases were separated by filtration. The solid hydrochar was dried at 100 °C for 24 h, then ground and sieved to 212-500 µm particle size. The hydrochar yield was 50.2 % (dry basis), and this hydrochar is hereafter referred to as H200. H200 was subsequently pyrolyzed in a tube furnace under N_2 atmosphere. A quartz boat containing 5 g of H200 was heated at 10 °C min^{-1} to the target temperature (350 °C or 550 °C), then allowed to cool to room temperature under N_2 flow. The resulting pyrochars were designated as PMB350 and PMB550, corresponding to their

pyrolysis temperatures. The pyrochar yield (dry basis) was 51.4 % for PMB350 and 44.7 % for PMB550, respectively.

2.2 Biochar Characterization

Various analytical techniques were employed to characterize the physicochemical properties of the biochar. The pH of each biochar was measured by dispersing 0.5 g of biochar in 50 mL of distilled water, stirring for 24 h, then filtered and measuring the filtrate using a calibrated pH meter (S470-K, Mettler Toledo, Switzerland). Specific surface area was determined from nitrogen adsorption–desorption isotherms (Autosorb IQ, Quantachrome, USA). The Brunauer-Emmett-Teller (BET) method was used to calculate the surface area, and the Barrett-Joyner-Halenda (BJH) method to determine pore size distribution. Elemental composition (C, H, N, S, and O) was determined using an elemental analyzer (FlashSmart CHNS/O, Thermo Fisher Scientific, USA). Proximate analysis was conducted according to a standard Korean waste testing method to determine moisture content (MC), volatile matter (VM), fixed carbon (FC), and ash content. Surface functional groups were identified using Fourier transform infrared spectroscopy (FT-IR, INVENIO, Bruker, Germany) over a wavenumber range of 4000-400 cm^{-1}. Surface elemental composition and chemical states were examined by X-ray photoelectron spectroscopy (XPS, Theta Probe, Thermo Fisher Scientific, UK) with spectra referenced to the C 1s peak at 284.8 eV. Peak fitting was performed using XPSPeak41 software, applying a Shirley background correction and Gaussian-Lorentzian peak shapes. Deconvolution of high-resolution S 2p spectra was performed using a doublet separation constraint of 1.18 eV and an area ratio of 2:1 for the S $2p_{2/3}$ and S2 $p_{1/2}$ components.

2.3 Odor Adsorption Experiments

As shown in Fig. 2, fixed-bed gas adsorption tests were carried out in a stainless-steel column (inner diameter 1.28 cm, height 20 cm) packed with 0.5 g of biochar sample. This packing resulted in bed heights of 1.80 cm for PMB350 (bulk density: 0.22 g cm^{-3}) and 1.02 cm for PMB550 (bulk density: 0.38 g cm^{-3}). The inlet gas flow was controlled with mass flow controllers (MFCs). The empty bed contact time (EBCT) of PMB350 and PMB550 was 1.39 s and 0.79 s, respectively. All gas-contacting components (tubing, fittings) were made of PTFE (Teflon) to minimize wall adsorption. Adsorption experiments were performed at ~25 °C (room temperature).

For single-gas experiments, either NH_3 (100 ppm in N_2) or H_2S (100 ppm in N_2) was fed to the column at 100 mL min^{-1}. For mixed-gas experiments, a mixture of NH_3 (100 ppm) and H_2S (100 ppm) in N_2 was supplied at a total flow of 100 mL min^{-1}.

For layered configurations, two pyrochar samples were sequentially packed (0.25 g each) in the column. The notation PMB350-550 indicates that the inlet gas first contacted PMB350 and subsequently PMB550, whereas PMB550-350 represents the reverse arrangement. The equal mass configuration was adopted to maintain the same total adsorbent mass in the single-bed experiments (0.5 g), enabling direct comparison between single and layered systems without introducing differences arising from adsorbent quantity. Due to the different bulk densities of the two pyrochars, equal mass packing inherently produced different layer thicknesses and residence times, which were treated as material dependent characteristics rather than independent design variables.

Accordingly, the interlayer interface was considered a reaction transition region along the flow direction, where chemical species generated in the upstream layer could influence reactions in the downstream layer, allowing evaluation of spatially coupled adsorption functions.

The outlet gas periodically sampled in Tedlar bags and analyzed using an H_2S/NH_3 analyzer (Model 30r-Ep, Los Gatos Research, USA). Each run continued until the outlet concentration equaled the inlet concentration ($C_{out}/C_{in} = 1$).

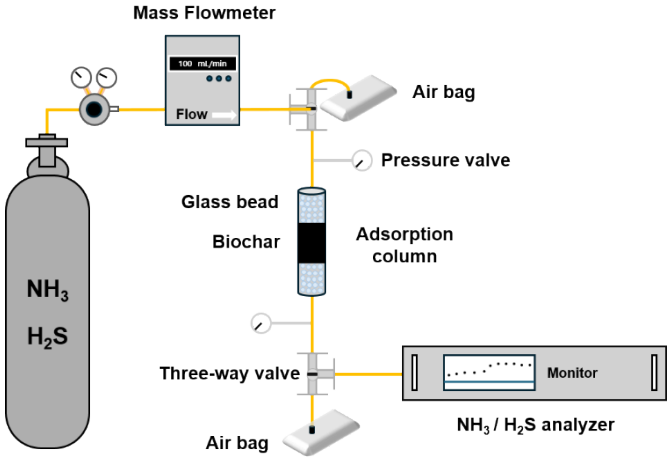

Fig. 2. Schematic diagram of gas adsorption apparatus.

2.4 Adsorption Capacity Calculation

Breakthrough curves (C/C_0 vs Time) were recorded for each adsorption test. The breakthrough time (t_b) was defined as the time when the outlet concentration (C) reached 10 % of the inlet concentration (C_0), while the saturation time (t_s) was when C/C_0 reached 0.95. The total adsorption capacity (q_t, mg g^{-1}) was calculated from the according to Eq. (1):(Zhao et al. 2022a)

$$q_t = (Q \times C_0)/m \int_0^{t_s} (1 - \frac{C}{C_0}) dt \quad \textit{Eq. (1)}$$

Where, q_t is the total adsorption capacity (mg g^{-1}), Q is the inlet flow rate (L min^{-1}), C_0 is the inlet concentration (mg L^{-1}), C is the outlet concentration as a function of time (mg L^{-1}), m is the mass of the adsorbent (g), and t_s is the saturation time (min)

3. Results and Discussion

3.1 Characterization of Pyrochar

3.1.1 Textural and Elemental Properties

Key physicochemical properties of PMB350 and PMB550 are summarized in Table 1. Increasing the pyrolysis temperature from 350 to 550 °C increased the BET surface area (from 27.9 to 90.0 m^2 g^{-1}) and total pore volume (from 0.1 to 0.2 cm^3 g^{-1}), while decreasing the average pore diameter (from 14.7 to 7.3 nm), indicating a shift toward smaller pores within the mesopore range. Both pyrochars were alkaline; pH increased from 8.59 (PMB350) to 9.80 (PMB550). These trends are consistent with previous studies on swine-manure-derived biochars which also reported that higher pyrolysis temperatures promote surface area development, smaller pore size, and increased alkalinity (Gasco et al. 2016). However, the surface area of PMB550 (90.0 m^2g^{-1}) was higher than the typical value (<50 m^2g^{-1}) reported for raw swine-manure chars (Cantrell et al. 2012). This is likely due to HTC pretreatment facilitating pore development by partially removing inorganic phases. Indeed, earlier reports have noted that coupling HTC with pyrolysis can enhance the surface area of the resulting char compared to direct pyrolysis alone (Arauzo et al. 2022).

Elemental analysis showed that both pyrochars had similar carbon contents (24.1-24.8 % C), but the higher-temperature char had lower hydrogen and oxygen contents. Between 350 °C and 550 °C, the H/C atomic ratio fell from 1.0 to 0.6 and the O/C ratio from 0.4 to 0.3 (Table 1). These declines indicate greater aromaticity and carbon stability at 550 °C, consistent with prior reports on swine-manure-derived biochar (Gascó et al. 2018).

Table 1. Physicochemical properties of PMB350 and PMB550

Sample	PMB350	PMB550

BET analysis results		
Surface area (m^2g^{-1})	27.9	90.0
Pore volume (cm^3g^{-1})	0.1	0.2
Pore size (nm)	14.7	7.3
Element analysis results		
C (%)	24.8	24.1
H (%)	2.1	1.1
N (%)	2.3	2.0
S (%)	0.9	1.0
O (%)	13.1	11.1
H/C ratio	1.0	0.6
O/C ratio	0.4	0.3
Proximate analysis (dry weight %)		
VM	25.0	16.0
FC	16.7	18.0
ash	58.3	66.0
pH	8.6	9.8

Proximate analysis results indicated that a greater loss of volatile occurred in PMB550 compared to PMB350. In contrast, PMB550 had an ash content of 66 %, about 8 % higher than that of PMB350. The increased specific surface area, pore volume, and ash content in high temperature pyrochar indicate that PMB550 has increased accessibility of mineral/alkaline sites, which are beneficial for H_2S adsorption.

3.1.2 Surface Functional Groups (FT-IR)

Fig. 3 shows the FT-IR spectra of PMB350 and PMB550. Both biochars exhibit prominent bands for O-H (broad ~3200-3600 cm^{-1}), aliphatic C-H (2800-3000 cm^{-1}), C=O (~1700 cm^{-1}), O-H bending (~1410 cm^{-1}), and C-O stretching (~1200 cm^{-1} and ~1080 cm^{-1}). These functional group bands were generally weaker for PMB550 compared to PMB350, reflecting the loss of oxygen-containing functional groups at higher pyrolysis temperature. Notably, the O-H (~3400 cm^{-1}), aliphatic C-H (~2900 cm^{-1}), and C=O (~1700 cm^{-1}) peaks were markedly reduced in PMB550, indicating decomposition of aliphatic moieties and removal of acidic surface groups. In summary, the FTIR analysis shows that higher pyrolysis temperature leads to a pronounced reduction in oxygen-containing functional groups (hydroxyls, carboxyls, carbonyls), as the biochar structure becomes more aromatic and carbonized. The higher density of reactive oxygen functional groups in PMB350 is favored for the adsorption of polar species like NH_3.

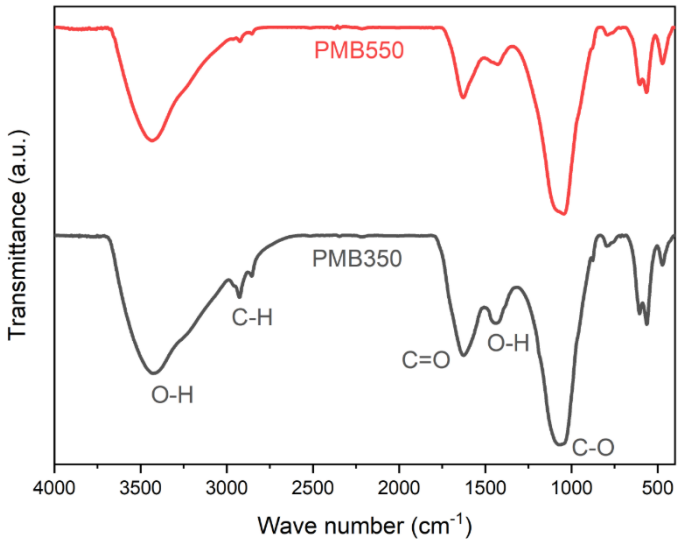

Fig. 3. FT-IR spectra of PMB350 and PMB550

3.2. NH_3 Adsorption Performance

The NH_3 adsorption breakthrough results for single-layer and layered beds are summarized in Table 2 and the corresponding breakthrough curves are presented in Fig. 4. In single-bed tests, the low-temperature pyrochar (PMB350) showed superior NH_3 removal performance compared to PMB550. PMB350 maintained a longer t_b and t_s (breakthrough at 233 min vs 180 min; saturation at 1,170 min vs 780 min), resulting in a higher NH_3 adsorption capacity of 7.10 ± 0.02 mg g^{-1}. This uptake was approximately 1.5 times greater than that of PMB550 (4.86 ± 0.06 mg g^{-1}). These differences indicate that the low-temperature biochar with more oxygenated functional groups provides more favorable NH_3 adsorption (likely via acid-base reactions forming surface NH_4^+).

By contrast, the layered bed (PMB350-550) did not improve overall NH_3 removal compared to the single materials. The layered bed showed an initial breakthrough at 197.6 min and reached saturation by 600 min, resulting in a total NH_3 capacity of only 4.01 ± 0.07 mg g^{-1}. This value is substantially lower than that of PMB350 alone (7.10 ± 0.02 mg g^{-1}) and even slightly below that of PMB550 (4.86 ± 0.06 mg g^{-1}). The lack of improvement can be attributed to the strong affinity of the front PMB350 layer for NH_3. With its abundance of oxygenated acidic functional groups (e.g., -COOH), the PMB350 layer readily captures NH_3 as NH_4^+, consuming the majority of NH_3 in the first half of the column. Consequently, the NH_3 concentration delivered to the downstream PMB550 layer was drastically reduced. Reducing the inlet NH_3 concentration is known to weaken the adsorption driving force in downstream sections of a fixed bed (Patel 2019; Rodrigues et al. 2007). Thus, although PMB550 has intrinsic capacity for NH_3 uptake, its contribution in the layered bed remained relatively lower.

Table 2. NH_3 adsorption performance for single-layer and layered beds.

Sample	t_b (min)	t_s (min)	q_t (mg g^{-1})
PMB350	233.1	1170.0	7.10 (± 0.02)
PMB550	180.0	780.0	4.86 (±0.06)

PMB350-550	197.6	600.0	4.01 (±0.07)

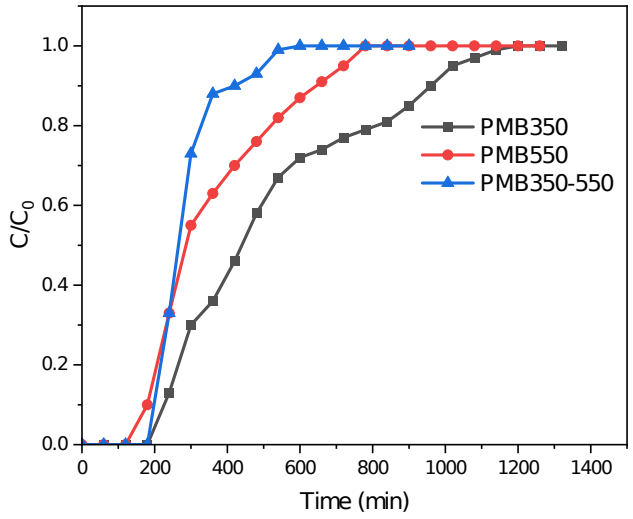

Fig. 4. Breakthrough curves of NH_3 on PMB350, PMB550 and PMB350-550

3.3 H_2S Adsorption Performance

In contrast to NH_3 results, the high-temperature biochar (PMB550) outperformed PMB350 for H_2S adsorption in single-gas tests. As shown in Table 3, PMB550 exhibited a t_b of 54 min and t_s of 1200 min, far exceeding those of PMB350 (t_b = 3.9 and t_s = 690 min). The corresponding adsorption capacity reached 9.70 ± 0.28 mg g^{-1}, nearly 3.8 times higher than that of PMB350 (2.54 ± 0.16 mg g^{-1}). The corresponding breakthrough curves are presented in Fig. 5.This confirms that the alkaline/mineral sites of high-temperature biochar play a dominant role in H_2S capture (Hervy et al. 2018). The accumulation of alkali components (Ca, Mg, and K) in PMB550, combined with its higher surface area and pore development, greatly increased H_2S-accessibile basic sites. These results highlight the intrinsic trade-off in optimizing biochar for single-gas adsorption: conditions favoring NH_3 uptake (low-temperature pyrochar with more acidic sites) are not optimal for H_2S, and vice versa. This motivates strategies such as layered configurations to integrate complementary properties for mixed-gas treatment.

In the layered bed (PMB350-550), the total H_2S adsorption capacity of 4.30 ± 0.35 mg g^{-1}, significantly higher than PMB350 alone (2.54 mg g^{-1}), but still well below that of PMB550 alone (9.70 mg g^{-1}). In the layered setup, the front PMB350 layer exhibits low inherent reactivity toward H_2S, so only limited fraction of H_2S was captured in the first layer. As a result, a relatively high H_2S partial pressure passed through the downstream PMB550 layer, which then captured H_2S effectively using its abundant basic surface sites. Overall, the layered bed exhibited contrasting behaviors for the two gases: NH_3 removal was hindered due to excessive upstream uptake in the first layer (reducing the driving force for the second layer), whereas H_2S removal benefited from complementary distribution of reactivity between layers. These results demonstrated that layered configurations can be advantageous, but their effectiveness strongly depends on the adsorption mechanism and chemical selectivity of each gas species.

Table 3. H_2S adsorption performance for single-layer and layered beds

Sample	t_b (min)	t_s (min)	q_t (mg g^{-1})

PMB350	3.9	690.0	2.54 (±0.16)
PMB550	54.0	1200.0	9.70 (±0.28)
PMB350-550	20.9	1050.0	4.30 (±0.35)

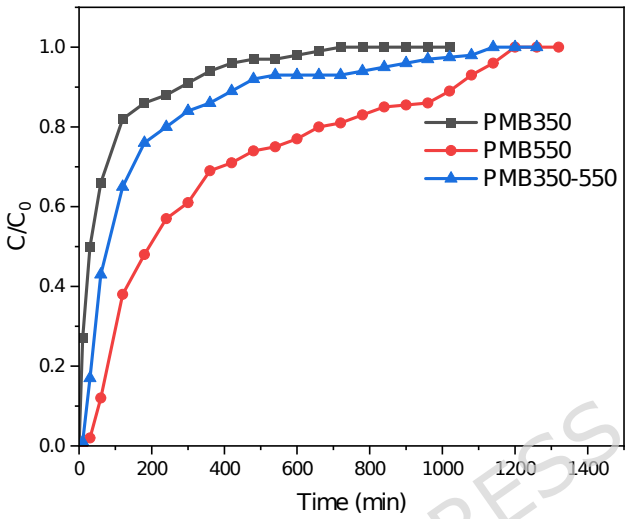

Fig. 5. Breakthrough curves of H_2S on PMB350, PMB550 and PMB350-550

3.4 Mixed NH_3/ H_2S Mixture Co-Adsorption in Layered Beds

The co-adsorption performance for NH_3/H_2S mixture in layered configurations (PMB350-550 vs. PMB550-350) is summarized in Table 4, and the corresponding breakthrough curve are shown in Fig. 6. Notably, NH_3 uptakes in the layered beds were slightly improved in the presence of H_2S. For the PMB350-550 configuration, the total NH_3 capacity was 4.31 ± 0.12 mg g^{-1}, marginally above the single-gas value of 4.01 ± 0.07 mg g^{-1}. A similar enhancement was observed for the reverse-layer bed (PMB550-350), where total NH_3 capacity reached 4.53 ± 0.04 mg g^{-1} (vs 4.86 mg g^{-1} PMB550 alone). These results suggest that NH_3 did not suffer competitive inhibition from H_2S; instead, the two gases interacted in a complementary manner within the columns.

One plausible interpretation is that a portion of H_2S is chemisorbed on the acidic sites of PMB350 and converted to HS^-/S^{2-} species. These anionic sulfur species would partially neutralize the strong acidic sites, thereby preventing the over-consumption of NH_3 in the front layer. In other words, with some acidic sites occupied by H_2S-drived species, the PMB350 layer may not scavenge NH_3 as completely as it did under single-gas case. This leaves a higher NH_3 partial pressure available for the downstream layer than under single-gas conditions, allowing a high driving force for NH_3 absorption in the second layer. Such behavior is consistent with prior observations that the presence of an acidic co-adsorbate can modulate the mass transfer zone in layered beds and mitigate the excessive uptake of basic gases in the front layer.

Under simultaneous exposure to NH_3 and H_2S, both layered configurations exhibited distinct adsorption behaviors compared with their single-gas performance, indicating complex competitive and sequential interactions. For H_2S in the mixture, the PMB350-550 bed achieved 7.15 ± 0.41 mg g^{-1}, while the PMB550-350 bed reached 7.60 ± 0.06 mg g^{-1}. These values are intermediate between the single-layer performances of PMB350 and PMB550, and significantly higher than layered-bed capacity for H_2S (4.30 mg g^{-1}) without

NH_3. Thus, under mixed-gas operation the presence of NH_3 enhanced the overall H_2S removal in the layered system by roughly 1.7-fold compared to the single-gas case. This synergistic improvement will be discussed mechanistically in the next section.

Table 4. Adsorption performance of NH_3/H_2S mixed gas on PMB350-550 and PMB550-350

Sample	Gas	t_b (min)	t_s (min)	q_t (mg g^{-1})	Synergy Assessment
PMB350-550	NH_3	211.0	690.0	4.31 (± 0.12)	Neutral
	H_2S	24.4	1170.0	7.15 (± 0.41)	Strong Synergy
PMB550-350	NH_3	207.0	660.0	4.53 (± 0.04)	Neutral
	H_2S	20.1	1350.0	7.60 (± 0.06)	Strong Synergy

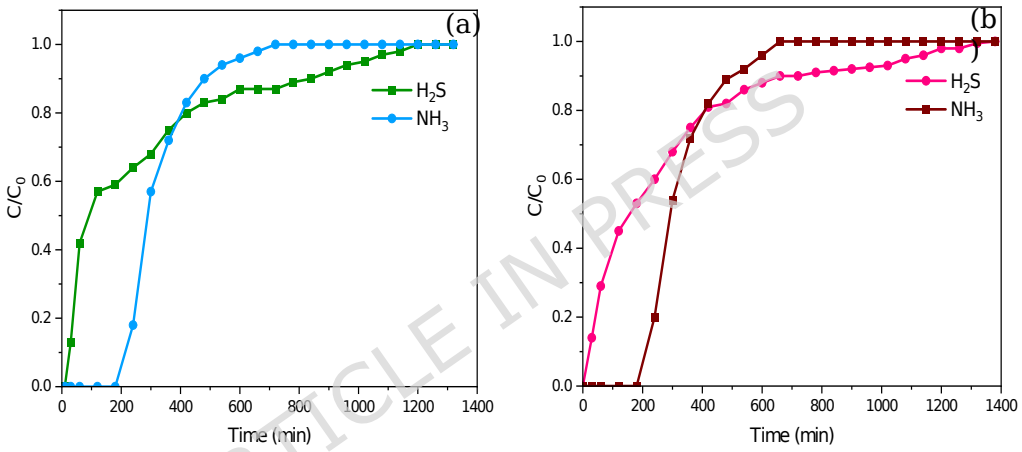

Fig. 6. Breakthrough curves of NH_3 and H_2S for the NH_3/H_2S mixed gas: (a) PMB350-550 and (b) PMB550-350

3.5 Mechanistic Insights into NH_3/H_2S Synergy

To elucidate the mechanism governing the enhanced H_2S removal in the mixed-gas layered system (PMB350-550), the surface chemical states of nitrogen, calcium, and sulfur were analyzed via XPS (Fig. 7 and Fig. 8). The data indicate that the presence of NH_3 induces a fundamental redistribution of the H_2S capture zones and oxidation pathways across the layered column, driven by cooperative acid-base interactions.

In the single-gas H_2S configuration (the left columns in Fig. 6 and Fig. 7), the upstream PMB350 layer exhibited moderate sulfur accumulation (Total S Area: 2,663 a.u.), with sulfur speciation distributed between elemental sulfur (S^0, 38.1 %) and sulfate (SO_4^{2-}, 41.3 %). The dominance of these species suggests that even without NH_3, the oxygen-rich surface of PMB350 facilitates partial oxidation. Upon the introduction of NH_3 in the mixed-gas stream, the total sulfur retention in the PMB350 layer increased by approximately 23 % (Total S Area: 3,279 a.u.). Contrasting the expectation of competitive inhibition, the speciation data reveals a shift towards higher oxidation states. The fraction of sulfate increased to 48.0 %, while the sulfide (S^{2-}) fraction contracted from 8.8 % to 2.1 %. This suppression of reduced sulfur species and the concomitant rise in sulfate indicate that co-adsorbed NH_3 acts as a promoter for H_2S oxidation.

This behavior can be attributed to the in-situ alkalinization of the surface. The N 1s spectra confirms the formation of ammonium (NH_4^+) on the PMB350 surface. The local increase in surface basicity facilitates the dissociation of H_2S into HS^- ions. The HS^- is a stronger nucleophile than molecular H_2S and is more susceptible to electrophilic attack by surface oxygen groups. Thus, the upstream layer functions not merely as an adsorbent but as a catalytic pre-oxidation zone, converting H_2S into stable sulfates and reducing the molar load reaching the downstream layer.

The most profound synergistic effect was observed in the downstream PMB550 layer (Fig. 7). Under mixed-gas conditions, the total sulfur content in this layer increased by a factor of 3.2 compared to the equivalent position in a single-gas run (S Area: 8,434 vs. 2,640 a.u.). The speciation in the PMB550 layer was dominated by elemental sulfur (41.0 %) and sulfate (35.1 %). Crucially, the Ca 2p spectra revealed a significant association between calcium and sulfate species. In the mixed-gas spent PMB550, $CaSO_4$ accounted for 53.4 % of the total Ca, compared to 48.5 % in the single-gas baseline. The PMB550 material, characterized by high ash content (66 %) and larger surface area (90.0 $m^2\ g^{-1}$), utilizes its alkaline earth mineral sites to fix oxidized sulfur species. The massive increase in sulfur uptake in the presence of NH_3 suggests that the base-catalyzed oxidation initiated in the first layer, combined with the continuous supply of residual NH_3 to the second layer, maximizes the utilization of these mineral sites. NH_3 likely facilitates the surface transport of acidic sulfur species to the basic mineral centers, enabling the formation of insoluble $CaSO_4$. The Ca 2p spectrum of the PMB550 layer showed that $CaSO_4$ (calcium sulfate) comprised a larger fraction of calcium-containing species when NH_3 was present (rising from ~53 % of Ca in the single- H_2S case to ~59 % under mixed gas). This confirms that NH_3 promoted a more extensive Ca-based sulfation reaction in the downstream layer, locking up sulfur as insoluble $CaSO_4$ (Hervy et al. 2018; Huang et al. 2022). Overall, the upstream acidic layer (PMB350) utilizes NH_3 to enhance the oxidative scrubbing of H_2S, preventing rapid breakthroughs. The downstream basic layer (PMB550) then functions as a high-capacity reservoir, where residual H_2S is efficiently mineralized. This challenges the conventional view that acidic and basic gases merely compete for sites; instead, the surface acid-base interactions can catalytically promote the removal of the co-pollutant.

From an operational perspective, the layered column can be interpreted as a system with spatially differentiated reaction functions rather than a uniform adsorption bed. Incoming NH_3 is preferentially captured in the upstream PMB350 layer, forming surface NH_4^+ and increasing local basicity, which shifts the H_2S reaction pathway toward dissociative and oxidative transformation. This behavior suggests that the upstream layer functions not merely as a storage region but as a reaction-conditioning zone that alters the chemical state of incoming reduced sulfur species. In the downstream PMB550 layer, the increased formation of Ca-associated sulfate indicates stabilization of sulfur species on mineral-based alkaline sites, implying a subsequent fixation step following upstream activation. This sequential distribution of functions disperses the removal process along the bed length and accounts for the delayed breakthrough and enhanced H_2S capacity observed under mixed-gas conditions.

Unlike a single-layer bed where removal primarily occurs within a moving mass-transfer zone, the layered configuration spatially separated activation and fixation processes. Consequently, NH_3 does not simply compete for adsorption sites but acts as a chemical regulator that modifies the reaction pathway and improves overall sorbent utilization along the column.

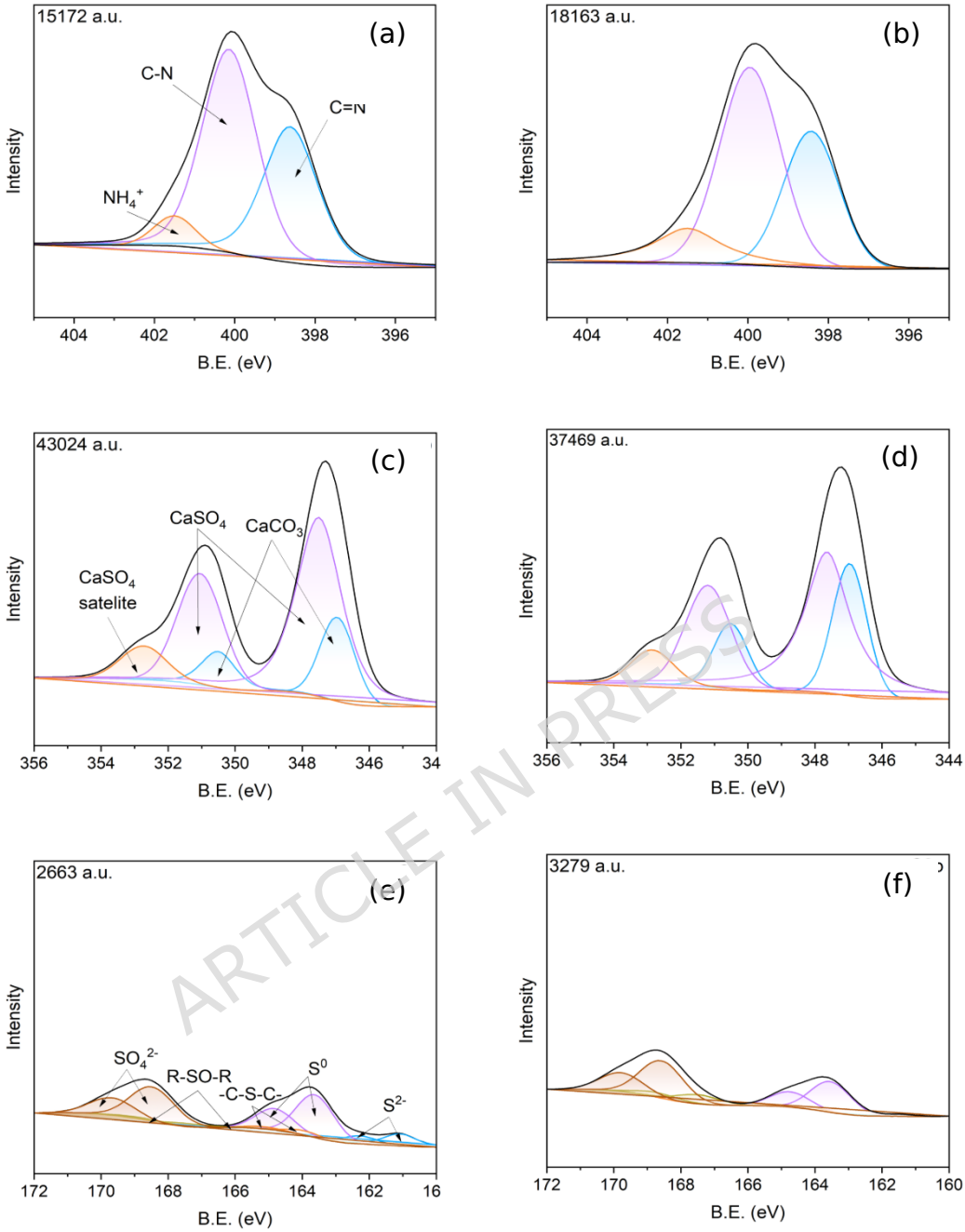

Fig. 7. XPS N 1s, Ca 2p and S 2p spectra of the PMB350 layer in the spent PMB350-550 beds under H_2S-only and mixed H_2S/NH_3 exposure. (a), (c), and (e) correspond to the N 1s, Ca2p, and S2p spectra of PMB350 under H_2S-only conditions, respectively; (b), (d), and (f) correspond to the N 1s, Ca 2p, and S 2p spectra of PMB350 under H_2S/NH_3 conditions.

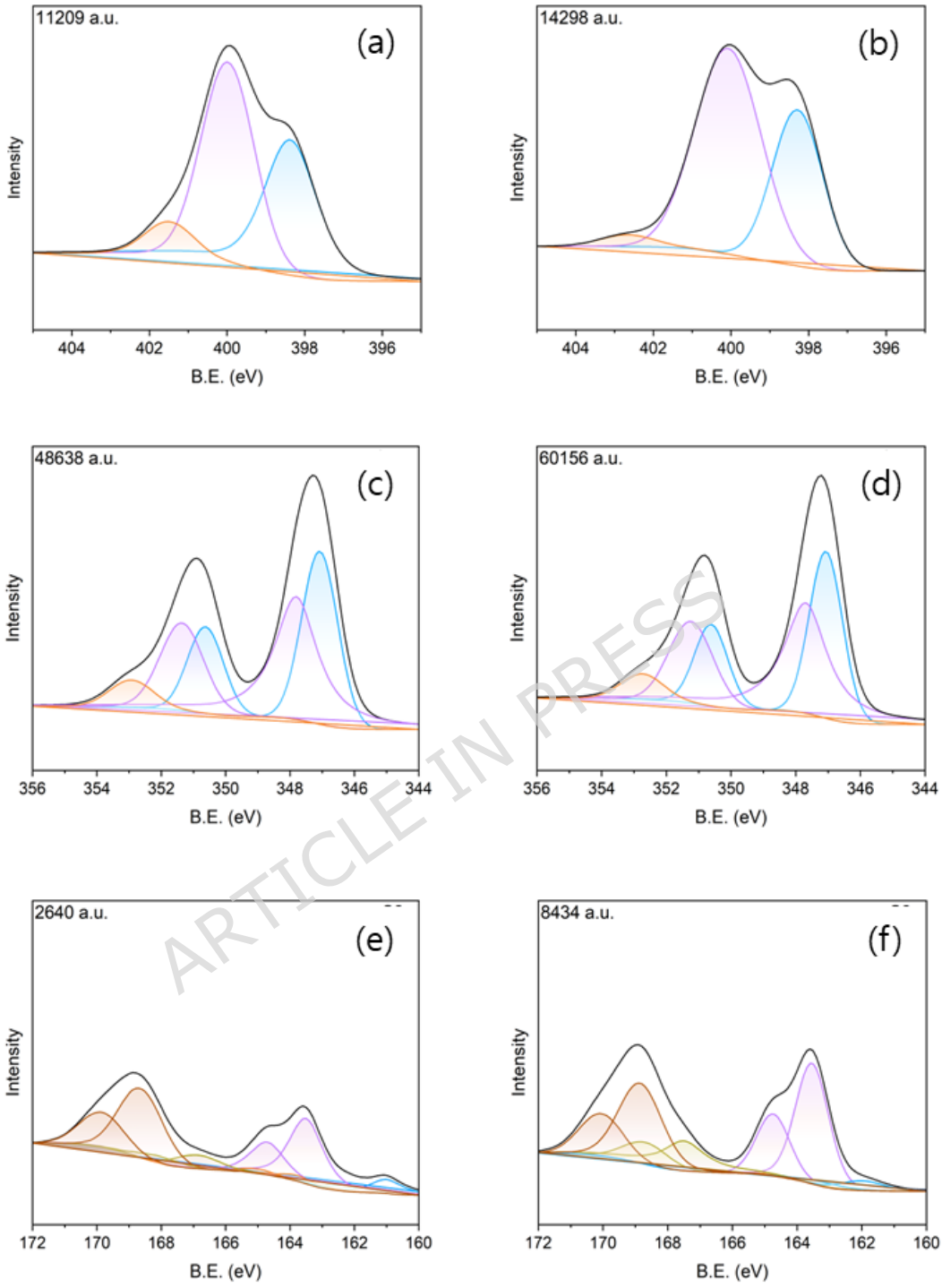

Fig. 8. XPS spectra of N 1s, Ca 2p and S 2p of the PMB550 layer in the spent PMB350-550 beds under H_2S-only and mixed H_2S/NH_3 exposure. (a), (c), and (e) correspond to the N 1s, Ca2p, and S2p spectra of PMB550 under H_2S-only conditions, respectively; (b), (d), and (f) correspond to the N 1s, Ca 2p, and S 2p spectra of PMB550 under H_2S/NH_3 conditions.

3.6. NH_3 Adsorption Mechanism

For completeness, XPS results for nitrogen on spent sorbents were analyzed to confirm the NH_3 adsorption mechanism as presented in Fig. 9. After NH_3 adsorption, both chars showed the appearance or growth of an N 1s signal corresponding to ammonium (NH_4^+, binding energy ~401- 402 eV). The NH_4^+ N 1s peak accounted for 14-15 % of total N 1s in NH_3-exposed samples for both PMB350 and PMB550, whereas only minor contributions were observed in the pristine sample (2.7 % for PMB350 and 4.6 % for PMB550). This strong signal indicates that NH_3 was primarily captured via Brønsted acid–base reactions, wherein surface acidic groups donate protons to NH_3 to form surface ammonium ions (NH_4^+) (Blanco et al. 2019). The detailed XPS spectra of C1s and O 1s are provided in Fig. 10. Consistently, the C 1s spectra of the chars showed a decrease in the C-O (alcohol/ether) peak and an increase in the O-C=O (carboxylate) peak after NH_3 adsorption, and the O 1s spectra showed a decrease in C–O and an increase in O-C=O. These changes support a mechanism in which NH_3 uptake involves deprotonation of carboxylic (or similar acidic) surface groups to form carboxylate salts with NH_4^+, as has been observed in prior studies (Blanco et al. 2019). The higher NH_3 adsorption capacity on PMB350 is largely attributable to its greater initial abundance of such acidic functional groups capable of proton transfer.

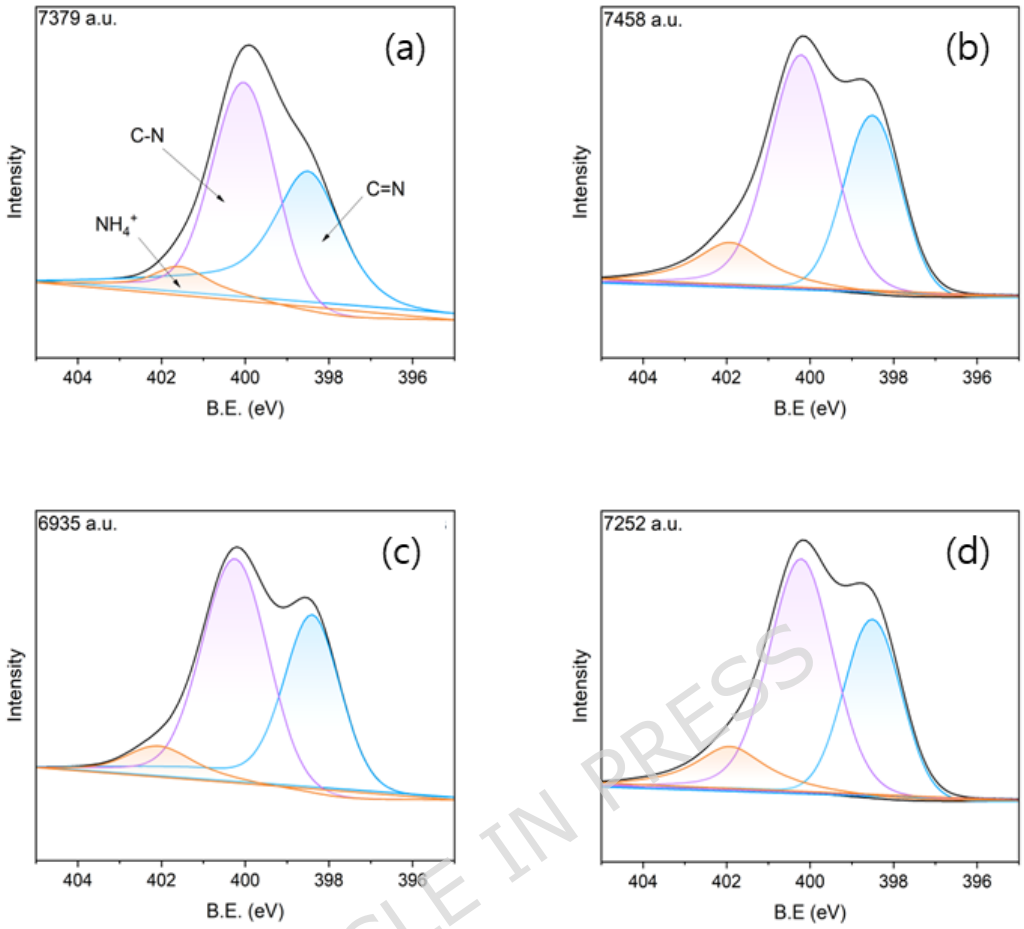

Fig. 9. XPS spectra N 1s spectra of PMB350 and PMB550 before and after being exposed to single NH_3. (a) PMB350 and (c)PMB550 before exposure; (b) PMB350 and (d) PMB550 after exposure.

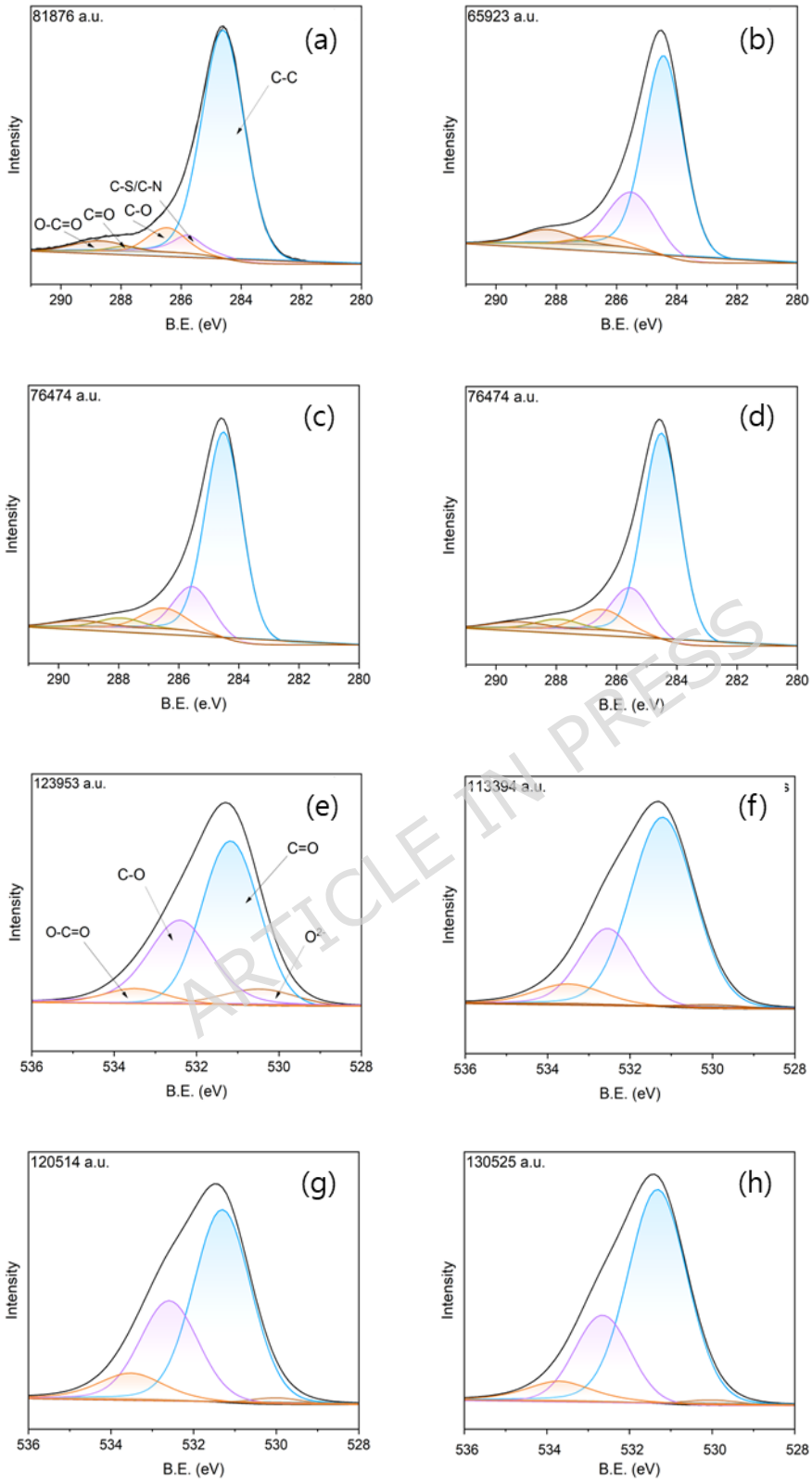

Fig. 10. XPS spectra C 1s and O 1s of PMB350 and PMB550 before and after single NH_3 exposure. C 1s spectra of PMB350 (a) before (b) after exposure; C 1s spectra of PMB550 (c) before and (d) after exposure; O 1s spectra of PMB350

(e) before and (f) after exposure; O1s spectra of PMB550 (g) before and (h) after the exposure.

3.7. Practical Implications and Environmental Significance

The present findings have important scientific and practical implications for controlling mixed NH_3-H_2S emissions using waste-derived adsorbents. By leveraging swine manure as a feedstock for hydrothermal carbonization (HTC) followed by pyrolysis, this study demonstrates a sustainable "waste-to-resource" approach: the problematic waste itself is converted into a functional sorbent capable of mitigating its own malodorous gases. The ability of swine-manure biochars to effectively adsorb NH_3 and H_2S under dry, inert conditions underscores their potential as low-cost alternatives to specialized commercial media.

In particular, simultaneous removal of an acidic gas (H_2S) and a basic gas (NH_3) is traditionally challenging, often requiring separate scrubbing steps or multiple sorbents, because these pollutants exhibit opposing chemistries (Jiang et al. 2022). Our findings reinforce the idea that inexpensive chars prepared from biomass waste can be engineered into efficient adsorbents for air purification. In practice, layered-biochar beds could be deployed in livestock barns, composting halls, or industrial exhaust systems to mitigate odor and toxic gas emissions. The concept of spatially segregating sorbent functions within one bed could also inspire new designs of multi-stage filters for other mixed emissions. Thus, the implications extend to other scenarios where complex gas mixtures must be cleaned: the methodology of layering different sorbents offers a flexible platform for multi-pollutant control across environmental engineering applications.

It is important to acknowledge the limitations of this study and the need for further research before field implementation. All experiments were conducted under idealized dry, air-free conditions (using N_2 as a balance gas). While this controlled atmosphere was useful for isolating intrinsic sorbent-gas interactions, real-world emissions are seldom dry or devoid of oxygen. Moisture in the gas stream can significantly influence adsorption processes (Sun et al. 2018). In some cases, the presence of water vapor may compete with or block adsorption sites; in others, humidity can enhance removal by dissolving gases into water films or by promoting certain reactions. For instance, recent work with mineral-rich biochars showed that adding 20 % moisture to the sorbent and a small O_2 concentration boosted H_2S capture by nearly an order of magnitude (from ~1.75 to 12.5 mg g^{-1}) because moisture and oxygen together facilitated oxidative conversion of H_2S to surface sulfate (Huang et al. 2022). Such dramatic moisture/O_2 synergy, as well as the inhibitory effects of coexistent gases like CO_2, were not examined in our dry N_2-based tests. Oxygen levels will also alter the chemistry: even a low O_2 content in exhaust air could accelerate the formation of sulfate or other oxidized species on the char surface (Sitthikhankaew et al. 2014). Additionally, real emissions feature fluctuating gas concentrations and flow rates rather than steady 100 ppm feeds. The performance of the layered bed under transient or low-concentration conditions (e.g. periodic spikes of H_2S or diurnal changes in NH_3 levels) remains to be evaluated.

5. Conclusion

This study demonstrates that layered biochar systems produced from swine manure via hydrothermal carbonization (HTC)-assisted pyrolysis can effectively remove NH_3 and H_2S under dry, air-free conditions. Removal performance was temperature dependent: PMB350 showed higher NH_3 capacity (7.10 mg g^{-1}) because its oxygenated acidic functional groups facilitated chemisorption as NH_4^+. PMB550 showed higher H_2S capacity (9.70 mg g^{-1}), consistent with more alkaline/mineral surface sites combined with its larger surface area (90.00 m^2 g^{-1}) and enhanced mesoporosity. Under mixed NH_3-H_2S feeds, the PMB350-550 layered bed exhibited synergistic H_2S control, raising total H_2S removal to 7.15 mg g^{-1} (1.7-fold) compared with the single-gas H_2S case (4.30 mg g^{-1}).

XPS results indicate that the presence of NH_3 induced a fundamental redistribution of the H_2S capture zones and oxidation pathways across the layered column, driven by cooperative acid-base interactions. Overall, the layered architecture provides a low-cost, catalyst-free approach to spatially program gas-solid interactions-intermediate trapping in the first layer followed by permanent sulfate fixation in the second - rather than simply combining two sorbents with different properties. Future work should assess regenerability, validate performance under field-relevant conditions, and optimize layer order, thickness, and property gradients to advance practical multi-pollutant odor control systems for livestock and industrial applications.

Author's contributions

All authors contributed to the study conception and design. Material preparation, data collection, and analysis were performed by Myeongjin Ko and Jae Hac Ko. The first draft of the manuscript was written by Myeongjin Ko and all authors commented on previous versions of the manuscript. All authors read and approved of the final manuscript.

Declarations

The datasets used or analyzed during the current study are available from the corresponding author upon reasonable request.

Funding: This research was supported by the Regional Innovation System & Education (RISE) program (2025-RISE-17-001) through the Jeju RISE center, funded by the Ministry of Education (MOE) and the Jeju Special Self-Governing Province, Republic of Korea and by Basic Science Research Program (RS-2023-00239414) through the National Research Foundation (NRF) funded by the Ministry of Education.

Acknowledgements: This research was supported by the Regional Innovation System & Education (RISE) program (2025-RISE-17-001) through the Jeju RISE center, funded by the Ministry of Education (MOE) and the Jeju Special Self-Governing Province, Republic of Korea and by Basic Science Research Program (RS-2023-00239414) through the National Research Foundation (NRF) funded by the Ministry of Education.

Competing interests

- The authors have no relevant financial or non-financial interests to disclose.
- The authors have no competing interests to declare that are relevant to the content of this article.
- All authors certify that they have no affiliations with or involvement in any organization or entity with any financial interest or non-financial interest in the subject matter or materials discussed in this manuscript.
- The authors have no financial or proprietary interest in any material discussed in this article.

References

Arauzo P, Maziarka P, Schoder K, Pfersich J, Ronsse F, Kruse A (2022) Influence of sequential HTC pre-treatment and pyrolysis on wet food-industry wastes: Optimisation toward nitrogen-rich hierarchical carbonaceous materials intended for use in energy storage solutions. Sci Total Environ 816: 151648. https://doi.org/10.1016/j.scitotenv.2021.151648

Ayaz M, Muntaha ST, Baltrėnaitė-Gedienė E, Kriaučiūnienė Z (2025) Biochar and carbon-negative technologies: exploring opportunities for climate change mitigation. Biochar 7(1): 17. https://doi.org/10.1007/s42773-024-00421-3

Bhoria N, Basina G, Pokhrel J, Reddy KSK, Anastasiou S, Balasubramanian VV, AlWahedi YF, Karanikolos GN (2020) Functionalization effects on HKUST-1 and HKUST-1/graphene oxide hybrid adsorbents for hydrogen sulfide removal. J

Hazard Mater 394: 122565. https://doi.org/10.1016/j.jhazmat.2020.122565
Blanco YS, Topel Ö, Bajnóczi ÉG, Werner J, Björneholm O, Persson I (2019) Chemical equilibria of aqueous ammonium–carboxylate systems in aqueous bulk, close to and at the water–air interface. Phys Chem Chem Phys 21(23): 12434-12445. https://doi.org/10.1039/C9CP02449B
Cantrell KB, Hunt PG, Uchimiya M, Novak JM, Ro KS (2012) Impact of pyrolysis temperature and manure source on physicochemical characteristics of biochar. Bioresour Technol 107: 419-428. https://doi.org/10.1016/j.biortech.2011.11.084
Cavali M, Junior NL, de Sena JD, Woiciechowski AL, Soccol CR, Belli Filho P, Bayard R, Benbelkacem H, de Castilhos Junior AB (2023) A review on hydrothermal carbonization of potential biomass wastes, characterization and environmental applications of hydrochar, and biorefinery perspectives of the process. Sci Total Environ 857: 159627. https://doi.org/10.1016/j.scitotenv.2022.159627
de Oliveira LH, Meneguin JG, Pereira MV, do Nascimento JF, Arroyo PA (2019) Adsorption of hydrogen sulfide, carbon dioxide, methane, and their mixtures on activated carbon. Chem Eng Commun 206(11): 1533-1553. 10.1080/00986445.2019.1601627
DeCoste JB, Peterson GW (2014) Metal–Organic Frameworks for Air Purification of Toxic Chemicals. Chem Rev 114(11): 5695-5727. 10.1021/cr4006473
Fang J, Zhan L, Ok YS, Gao B (2018) Minireview of potential applications of hydrochar derived from hydrothermal carbonization of biomass. J Ind Eng Chem 57: 15-21. https://doi.org/10.1016/j.jiec.2017.08.026
Garlapalli RK, Wirth B, Reza MT (2016) Pyrolysis of hydrochar from digestate: Effect of hydrothermal carbonization and pyrolysis temperatures on pyrochar formation. Bioresource technology 220: 168-174.
Gascó G, Paz-Ferreiro J, Álvarez ML, Saa A, Méndez A (2018) Biochars and hydrochars prepared by pyrolysis and hydrothermal carbonisation of pig manure. Waste Manag 79: 395-403. https://doi.org/10.1016/j.wasman.2018.08.015
Gasco G, Paz-Ferreiro J, Cely P, Plaza C, Mendez A (2016) Influence of pig manure and its biochar on soil CO2 emissions and soil enzymes. Ecol Eng 95: 19-24. https://doi.org/10.1016/j.ecoleng.2016.06.039
Guo J, Luo Y, Lua AC, Chi R-a, Chen Y-l, Bao X-t, Xiang S-x (2007) Adsorption of hydrogen sulphide (H2S) by activated carbons derived from oil-palm shell. Carbon 45(2): 330-336. https://doi.org/10.1016/j.carbon.2006.09.016
Hervy M, Minh DP, Gerente C, Weiss-Hortala E, Nzihou A, Villot A, Le Coq L (2018) H2S removal from syngas using wastes pyrolysis chars. Chem Eng J 334: 2179-2189. https://doi.org/10.1016/j.cej.2017.11.162
Huang D, Wang N, Bai X, Chen Y, Xu Q (2022) The influencing mechanism of O2, H2O, and CO2 on the H2S removal of food waste digestate-derived biochar with abundant minerals. Biochar 4(1): 71.
Ighalo JO, Rangabhashiyam S, Dulta K, Umeh CT, Iwuozor KO, Aniagor CO, Eshiemogie SO, Iwuchukwu FU, Igwegbe CA (2022) Recent advances in hydrochar application for the adsorptive removal of wastewater pollutants. Chem Eng Res Des 184: 419-456. https://doi.org/10.1016/j.cherd.2022.06.028
Ipiales RP, Sarrion A, Diaz E, Diaz-Portuondo E, Mohedano AF, de la Rubia A (2023) Strategies to improve swine manure hydrochar: HCl-assisted hydrothermal carbonization versus hydrochar washing. Biomass Conv Bioref 13(18): 16467-16478. https://doi.org/10.1007/s13399-023-04027-w
Jiang Q, Li T, He Y, Wu Y, Zhang J, Jiang M (2022) Simultaneous removal of hydrogen sulfide and ammonia in the gas phase: a review. Environmental Chemistry Letters 20(2): 1403-1419.
Khabazipour M, Anbia M (2019) Removal of Hydrogen Sulfide from Gas Streams Using Porous Materials: A Review. Ind Eng Chem Res 58(49): 22133-22164. 10.1021/acs.iecr.9b03800
Maniscalco MP, Volpe M, Messineo A (2020) Hydrothermal Carbonization as a Valuable

Tool for Energy and Environmental Applications: A Review. Energies 13(16): 4098. https://doi.org/10.3390/en13164098
Marszałek M, Kowalski Z, Makara A (2018) Emission of greenhouse gases and odorants from pig slurry-effect on the environment and methods of its reduction. Ecol Chem Eng 25(3): 383-394. https://doi.org/10.1515/eces-2018-0026
Mohamed EF, El-Mekawy A, Ahmed SAS, Fathy NA (2024) High Adsorption Capacity of Ammonia Gas Pollutant Using Adsorbents of Carbon Composites. Arab J Sci Eng 49(1): 261-271. 10.1007/s13369-023-07987-3
Olszewski MP, Nicolae SA, Arauzo PJ, Titirici M-M, Kruse A (2020) Wet and dry? Influence of hydrothermal carbonization on the pyrolysis of spent grains. J Clean Prod 260: 121101. https://doi.org/10.1016/j.jclepro.2020.121101
Patel H (2019) Fixed-bed column adsorption study: a comprehensive review. Appl Water Sci 9(3): 45. https://doi.org/10.1007/s13201-019-0927-7
Pérez-Botella E, Valencia S, Rey F (2022) Zeolites in Adsorption Processes: State of the Art and Future Prospects. Chem Rev 122(24): 17647-17695. 10.1021/acs.chemrev.2c00140
Ravindiran G, Rajamanickam S, Janardhan G, Hayder G, Alagumalai A, Mahian O, Lam SS, Sonne C (2024) Production and modifications of biochar to engineered materials and its application for environmental sustainability: a review. Biochar 6(1): 62. https://doi.org/10.1007/s42773-024-00350-1
Rodrigues CC, de Moraes Jr D, Da Nobrega SW, Barboza MG (2007) Ammonia adsorption in a fixed bed of activated carbon. Bioresour Technol 98(4): 886-891. https://doi.org/10.1016/j.biortech.2006.03.024
Sitthikhankaew R, Chadwick D, Assabumrungrat S, Laosiripojana N (2014) Effects of humidity, O2, and CO2 on H2S adsorption onto upgraded and KOH impregnated activated carbons. Fuel Process Technol 124: 249-257. https://doi.org/10.1016/j.fuproc.2014.03.010
Song J-M (2024) Emission characteristics of odorous compounds from a swine farm on jeju island, Korea. Atmosphere 15(3): 327. https://doi.org/10.3390/atmos15030327
Su M, Li N, Huang T, Zhu B (2023) Competitive Interactions of NH 3 and Toluene with Biochar Modified by Pre-and Post-Treatments of H 3 PO 4 in Dual Adsorption Systems. BioResources 18(2). https://doi.org/10.15376/biores.18.2.3870-3884
Sun X, Ruan H, Song X, Sun L, Li K, Ning P, Wang C (2018) Research into the reaction process and the effect of reaction conditions on the simultaneous removal of H 2 S, COS and CS 2 at low temperature. RSC Adv 8(13): 6996-7004. DOI https://doi.org/10.1039/C7RA12086A
Wang T, Zhai Y, Zhu Y, Li C, Zeng G (2018) A review of the hydrothermal carbonization of biomass waste for hydrochar formation: Process conditions, fundamentals, and physicochemical properties. Renew Sustain Energy Rev 90: 223-247. https://doi.org/10.1016/j.rser.2018.03.071
Wang Y-C, Han M-F, Jia T-P, Hu X-R, Zhu H-Q, Tong Z, Lin Y-T, Wang C, Liu D-Z, Peng Y-Z (2021) Emissions, measurement, and control of odor in livestock farms: A review. Sci Total Environ 776: 145735. https://doi.org/10.1016/j.scitotenv.2021.145735
Zeng G, Guo S, Zhai X (2024) Experimental study on adsorption of SO2 and NH3 by activated carbon with monometallic active sites at low concentration under room temperature. ACS omega 9(5): 5523-5533. https://doi.org/10.1021/acsomega.3c07430
Zhao Y, Chen Y, Qian C, Wang H, Jiang H, Niu C, Gai J, Zhao Q, Lou Y, Shen B (2022a) Constructing AgY@ Cu-BTC hybrid composite for enhanced sulfides capture and moisture resistance. Micropor Mesopor Mat 341: 112043. https://doi.org/10.1016/j.micromeso.2022.112043
Zhao Z, Wang B, Theng BK, Lee X, Zhang X, Chen M, Xu P (2022b) Removal performance, mechanisms, and influencing factors of biochar for air pollutants: a

critical review. Biochar 4(1): 30. https://doi.org/10.1007/s42773-022-00156-z
Zhuang Z, Wang L, Tang J (2021) Efficient removal of volatile organic compound by ball-milled biochars from different preparing conditions. J Hazard Mater 406: 124676. https://doi.org/10.1016/j.jhazmat.2020.124676